Few-seconds range verification with short-lived positron emitters in carbon ion therapy

(Article begins on next page)

18 December 2024

Few-seconds range verification with short-lived positron emitters in carbon ion therapy

Caterina Cuccagna[1,2], Giuseppe Battistoni[3], Maria Giuseppina Bisogni[4,5],
Piergiorgio Cerello[6], Alberto Del Guerra[4], Veronica Ferrero[6,7], Elisa Fiorina[6],
Matteo Morrocchi[4,5], Francesco Pennazio[6], Roberto Sacchi[6,7] and UgoAmaldi[1]

[1]TERA Foundation, Novara, Italy
[2]DPNC, Université de Genève, Geneva, Switzerland
[3]INFN sezione di Milano, Italy
[4]Università di Pisa, Italy
[5]INFN sezione di Pisa, Pisa, Italy
[6]INFN sezione di Torino, Italy
[7]Università degli Studi di Torino, Torino, Italy

E-mail: caterina.cuccagna@outlook.com

Abstract

In-beam PET (Positron Emission Tomography) is one of the most precise techniques for in-vivo range monitoring in hadron therapy. Our objective was to demonstrate the feasibility of a short irradiation run for range verification before a carbon-ion treatment. To do so a PMMA target was irradiated with a 220 MeV/u carbon-ion beam and annihilation coincidences from short-lived positron emitters were acquired after irradiations lasting 0.6 seconds. The experiments were performed at the synchrotron-based facility CNAO (*Italian National Center of Oncological Hadrontherapy*) by using the INSIDE in-beam PET detector. The results show that, with $3 \cdot 10^7$ carbon ions, the reconstructed positron emitting nuclei distribution is in good agreement with the predictions of a detailed FLUKA Monte Carlo study. Moreover, the radio-nuclei production is sufficiently abundant to determine the average ion beam range with a σ of 1 millimetre with a 6 seconds measurement of the activity distribution. Since the data were acquired when the beam was off, the proposed rapid calibration method can be applied to hadron beams extracted from accelerators with very different time structures.

Keywords: in-beam PET, hadron therapy, range measurement, short-lived β+ emitters

1. Introduction

In the 90s at GSI[1] Helmholtz Centre, in-beam PET (Positron Emission Tomography) was employed for the first time to monitor the dose distributions in patients irradiated with pencil beams of carbon ions [1] [2]. Twenty years later, the technique is becoming a medical tool with the aim of verifying in-vivo the particle range [3] [4]. From the in-beam PET data, the hadron

---

[1] Gesellschaft für Schwerionenforschung

range in the patient body can be calibrated immediately *after a few minutes* treatment with millimetre precision, an accuracy that cannot be achieved by the standard method of computing the electron density– and thus the ion beam range – from CT images [5].

An in-beam PET range verification method that could be executed in less than 5-10 seconds, and immediately *before* the therapeutic irradiation, would be a most valuable tool in hadron therapy. In this work we present the measurements made at CNAO (the *Italian National Hadron therapy Centre in Pavia*) and prove that the range verification can be obtained using short-lived positron emitters produced in the nuclear interactions of carbon ions with human tissues.

At the ICTR-PHE2016 conference held in Geneva, two of the authors (U.A. and C.C.) proposed to detect *short-lived* positron emitting nuclei produced by a carbon ion beam, ready to treat a patient, in a small "calibration volume" inside the tumour target [6]. Monte Carlo simulations had been performed with the FLUKA code[7] [8] [9] to determine the individual contributions of the short-lived positron emitting isotopes to the overall β^+ emitters activity produced by the interaction of a ^{12}C pencil beam in a water phantom and evaluate their distribution in space and time. A *2 second run* was defined consisting in irradiating a water target of 6 cm^3 volume with $3 \cdot 10^7$ carbon ions for 0.6 s (corresponding to a delivered dose in the target of 0.2 Gy, i.e. 10% of a typical treatment dose), and acquiring the β^+ emitters activity in the following 1.4 s. The conclusions were that in this 2 second run, $6 \cdot 10^4$ Boron-8 nuclei would be produced, representing the main contributor to the β^+ emitters activity distribution and a PET detector with a 2% efficiency would detect 1200 coincidences resulting in a 1 mm range accuracy. The results of such a short "calibration run" could be used to correct the energy of the beam before delivering the required dose to the tumour target in the following "treatment run".

The experiments performed at CNAO and described in this paper prove that the method is applicable in a medical environment with the existing INSIDE in-beam PET scanner [10] [11].

2. Materials and methods

Experimental setup and data acquisition.

The INSIDE in-beam PET detector consists in two planar heads with 26.4 × 11.25 cm^2 area each. They are made of matrices of segmented Lutetium Fine Silicate (LFS) scintillating crystals, segmented into 16×16 elements of 3.2 mm pitch and coupled 1:1 to Hamamatsu Silicon PhotoMultipliers (SiPMs). Each head consists then of 2×5 modules, with 3.3 mm gaps in between. The distance between the two heads is 50 cm. All the signals from the 2×2560 pixels are acquired by a Front-End electronics based on the TOFPET ASIC and processed by 20 Xilinx SP605 FPGA boards [10] [11]. The efficiency of this detector is about 3%. For more details, the reader should consult the original publications [12] [13][14].

A homogeneous PMMA phantom of dimensions 4.9×4.9×20 cm^3 was irradiated with a mono-energetic carbon ion beam of E=222 MeV/u in a CNAO treatment room, where a horizontal beam is available. The irradiation with $3 \cdot 10^7$ carbon ions lasted 0.6 s. The PMMA phantom was positioned at the center of the FOV of the INSIDE scanner and PET signal acquired.

The data acquisition and the time-tagged PET image processing systems, developed by the INSIDE collaboration, allow the collection of PET coincidences and the optimal reconstruction of PET

2

images with five iterations of the MLEM (Maximum-Likelihood Expectation-Maximization) algorithm, without exploiting the Time of Flight information [15].

Filtering options are available both at the events level as well as at the image level.

For the counting of the number of coincidences over time *no energy filter* was applied, whereas - for the reconstruction of the 2D profiles - an energy window of ± 56keV around the channel of the photopeak at 511keV was defined. As discussed in Section 3, this cut reduced the fraction of background events, mainly due to the decay of Lutetium nuclei contained in the crystal, by a factor 4.

For the reconstruction, the obtained images were smoothed with a three-dimensional 'median filter' [16] [17] [18], with a kernel of 5 cm wide corresponding to 7×7×7 voxels. The effect of this filter is to remove salt-and-pepper noise while preserving the edges. An example of the effect on PET images, extracted from the experimental data collected in 231 s, irradiatiating with a mono-energetic carbon ion beam of E=222 MeV/u, is shown in the Figure 1. After the filtering, the sparse hits disappear, and the borders are much better defined. This 'median filter' greatly improves the determination of the particle range.
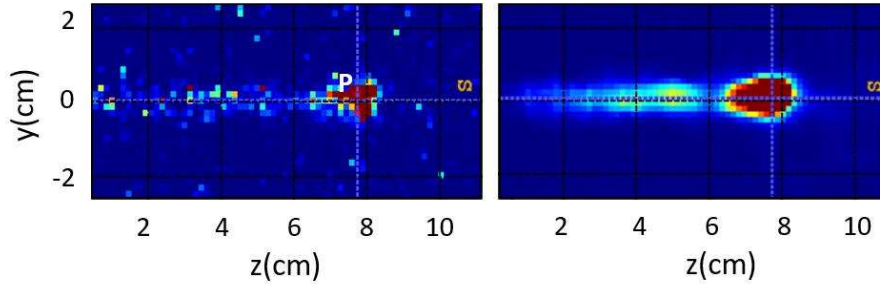

Figure 1. *Experimental data acquired for a total time of 231 s after irradiation with a mono-energetic carbon ion beam (E=222 MeV/u) incident in a PMMA target along z direction without (left) and with (right) the application of the median filter. P represents the crossing point between the blue vertical and horizontal axis, point of maximum intensity, cited later in the text.*

Monte Carlo simulations.

The accuracy of the measurements was evaluated performing 49 simulation runs, each one with $3 \cdot 10^7$ primary ^{12}C ions with an improved version of the INSIDE Monte Carlo (MC) simulation tool, following a *two steps* approach [19] [12]. The tool is based on the FLUKA MC code development version 2018, including, in addition to the state-of-the-art physics models embedded in FLUKA [20] [21], dedicated improvement for hadron therapy applications [22] [23] [7]. As specific settings of those simulations "PRECISIOn" card was used as DEFAULT setting. The experimental conditions of the irradiation of a single spot with a mono-energetic carbon ion beam of E=222 MeV/u were reproduced. In particular, the simulation tool includes the CNAO beam line elements, the primary beam characteristics with its temporal structure and the INSIDE detector geometry.

3

Moreover, the simulation runs were also post-processed with the same algorithms used to treat the experimental data.

To determine the main β^+-emitters produced in fragmentation events and contributing to the observed longitudinal peak, the temporal and spatial distributions of the MC simulated annihilations in the target were reconstructed, taking into account the parent isotopes. Table 1 summarizes the main β^+-emitters produced.

Isotope	$T_{1/2}$ (s)	nuclei/^{12}C (222 MeV/u) PMMA phantom V=4.90x4.90x20 cm³
^{15}O	122.24	1.27E-02
^{14}O	70	3.47E-04
^{13}N	597.9	1.80E-03
^{12}N	0.011	3.17E-04
^{11}C	1221.84	7.52E-02
^{10}C	19.29	3.93E-03
^{9}C	0.1265	5.03E-04
^{8}B	0.77	3.58E-03

Table 1. Production of positron-emitting isotopes in the irradiation with carbon ions of PMMA phantoms. The isotopes with yield smaller than 10^{-4} are omitted.

Figure 2 shows the activity and annihilation counts, summed over the 49 MC runs and integrated over time as functions of time. In addition to the four isotope with higher yield: ^{8}B, ^{10}C, ^{15}O ^{11}C, two isotopes with lower yield (^{12}N and ^{9}C) contribute to the integrated count in the first second.

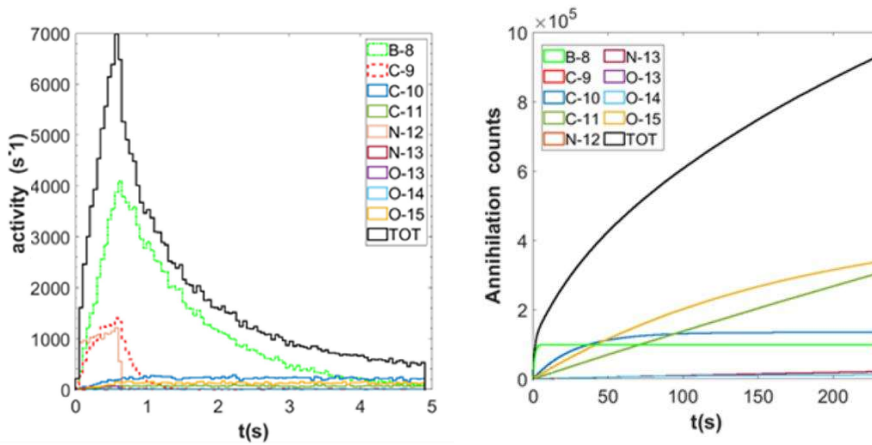***Figure 2.*** *Simulated activity of the main isotopes produced by 49 x 3·10⁷ radioisotopes delivered in a 0.6 s irradiation. Left: Acquisition time: 5 s with a 0.05 s binning. Right: Integrated number of counts in a 231 s acquisition from the end of the irradiation.*

4

Figure 3 shows the longitudinal distributions of the annihilation events along the beam direction z, reconstructed at different acquisition times, and gives the isotopes contributing to the fragmentation peak. The results confirm the dominance of ^8B nuclei during the short irradiation in the first 10 s that gives the main contribution to the activity, as obtained from the preliminary simulations in 2016.
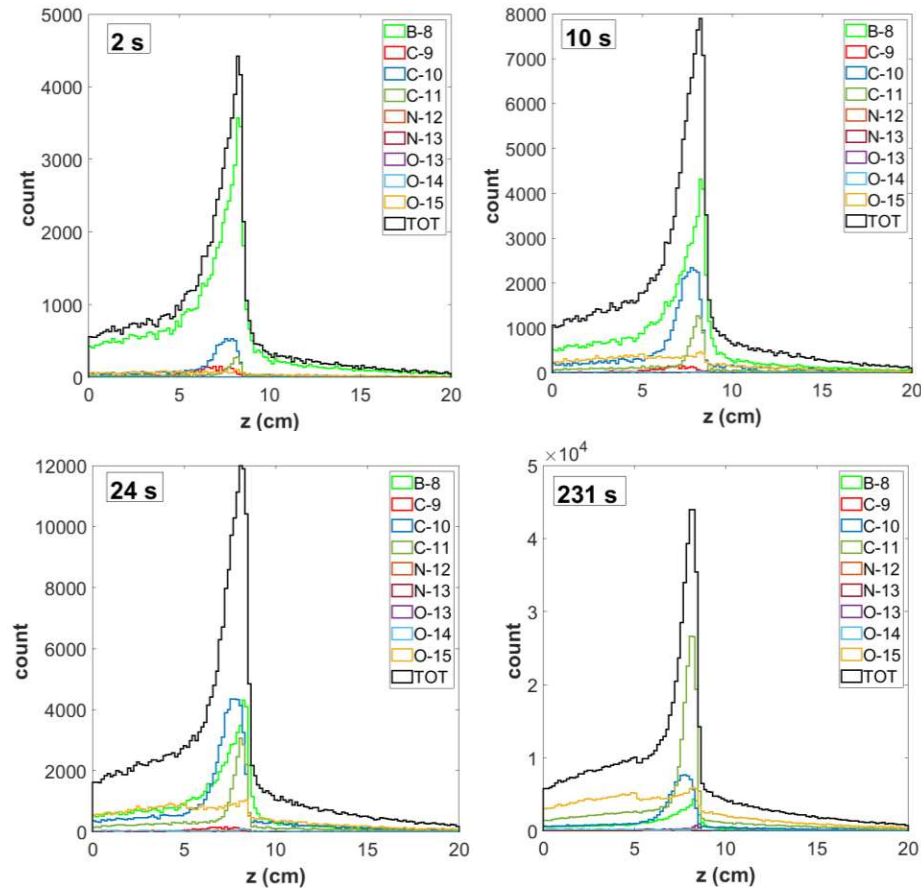

Figure 3. 1D profiles of the annihilations produced in the PMMA target at different acquisition times after the irradiation end (binning 1.6 mm).

5

Data Analysis

Data analysis tools were developed using the ROOT toolkit [24] and MATLAB® [25] with two complementary objectives in mind: (i) estimating the fractions of events due to each isotope, by using the time-dependence of the measured coincidence rate and (ii) determining the variation of the fragmentation peak characteristics as a function of time.

The first goal was attained by fitting simulated and measured coincidences rates with the exponential decays as a function of time. To this end, the total coincidences rate $C(t)$ as a function of the time t, measured from the end of the irradiation period, was written as

$$C(t) = \sum_{i=1}^{M} C_{o_i} \cdot e^{-\lambda_i t} \qquad (1)$$

where the quantities λ_i are the decay constants of each isotope i, M is the number of nuclei species that are abundantly produced and are thus included in the fit, and C_{o_i} are the coincidence rates of each isotope at the end of the 0.6 s irradiation time.

In the first analysis, applied to the whole target *without* either energy cuts on the detected photon signals or three-dimensional median filter, equation (1) has been used to fit MC simulated and experimental rates with C_{o_i} as free parameters.

In order to compare the data with the output of the MC runs, the measured constant rate background due to the decay of lutetium, contained in the LSF detector, has been considered [26]. The background distribution, determined by measurements done before the irradiation, is Poisson-like with a mean value of 51.0 coincidences per second with a variability of 0.9 coincidences per second.

The first data analysis was performed in four steps. As generally used in experiments with relatively low counting rates, where the Gaussian approximation of the Poisson statistics is no longer valid, a binned likelihood fitting method was applied [24][27][28]. The quality of the fit was determined by computing two parameters: Pearson's chi-square χ_P^2, and Baker-Cousins chi-square χ_{BC}^2 [29] .

First of all, a fit to the *average* of the 49 FLUKA runs was performed to estimate the fit parameters, without any artificially added background. The five isotopes giving the largest contributions were considered and they are: ^{9}C, ^{8}B, ^{10}C, ^{15}O, ^{11}C. Secondly, in order to quantify the precision of the estimated parameters, the 49 runs were fitted separately, obtaining the averaged fitting parameters with related errors. Thirdly, a background Poisson noise – with a mean value constant in time of (5.10±0.09) events per bin of 0.1 s - was added to each of the 49 MC runs. Each run was then fitted with a formula obtained by adding to equation (1) a constant value K=5.1 events/0.1 s. Finally, the same fitting equation was applied to the experimental data, by keeping the parameters which showing a larger uncertainty, fixed at the values determined with the Monte Carlo. The comparison of the output of these fits to the data and to the MC outputs allows an estimate of the production rates of the different β⁺-emitters.

In the second analysis, for the most important measurement - i.e. the determination of the range of the 222 MeV/u carbon ions, the following procedure was applied:

6

1. Sum the counts for various time intervals after the end of the irradiation for both the experimental data and the MC .

2. Application of the median filter to each data set, already filtered in energy.

3. Extraction of the 1D profiles along the z direction from the 3D images[2].

4. Comparison between the parameters resulting from the Gaussian fits of the data and the ones of the MC.

3. Results

Coincidences evolution versus time and isotopes contribution

The results of the first analysis are presented in Figure 4 and Table 2. Figure 4 shows the coincidence rate, expressed in number of events per bin of 0.2 s, together with a zoom of the first 28 s of acquisition. Three coincidence rate histograms are plotted: simulation, simulation with added noise (both simulated curves are the distributions of the results for the 49 runs) and experimental results. The corresponding fitted curves are also drawn.

The first important observation is that the experimental data are slightly (15%) larger than the MC predictions. In particular, the fitted parameters of equation 1, corresponding to the fractions of coincidences due to the main β^+ nuclei, are presented in Table 2 and allow to quantify these differences.

Column (a) contains the overall fit of the sum of the 49 runs, giving small errors due to high statistics. The χ^2 is close to 1.0, thus indicating a good fit. Since in this case the statistics are high, and therefore the Poisson distribution can be approximated with a Gaussian, also the Pearson's χ^2 is performing well. Column (b) shows the average of the fit parameters and the corresponding standard deviations σ obtained by fitting separately each one of the 49 runs. The central values match the ones in column (a) and the statistical errors are roughly 7 times larger, as expected because there are 49 MC runs.

The fit parameters shown in column (c), (d) and (e) were obtained fitting the data with the equation (1) modified in order to take into account the constant Poisson noise contribution. The resulting averaged parameters from the 49 separated fits of the simulation curves with added noise are shown in column (c).

In the column (d), the parameters coming from the same fits of column (c) are presented but fixing the two parameters for ^{15}O and ^9C. In this way, the fitting parameters of curves with noise are closer to the values in column (c). Finally, the results obtained by fitting the experimental data with the same equation are reported in column (e).

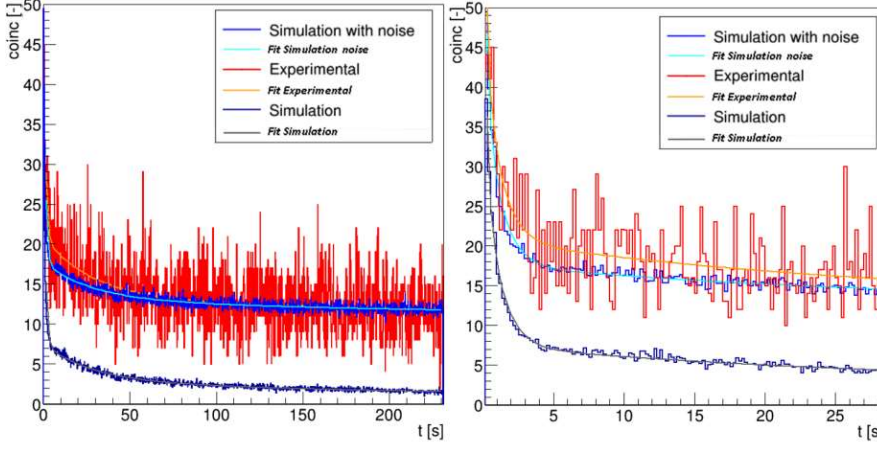[2] Profiles obtained summing the signal intensity over x and y

7

Figure 4. *Left : Experimental (red) versus the simulated (purple) coincidence rate (bin = 0.2 s), starting from the end of the irradiation during the next 231 s. The simulation curve with added noise is depicted in blue. The related fitting curves are also shown. Right: zoom of the first 28 s.*

Table 2. Parameters C_{o_i} of the fitting curves, representing the coincidences count rate over time (Eq. 1). Column a) and b) represent simulated data without noise. Columns c), d), simulated data with noise and column e) experimental data. The parameters fixed in column (d) and (e) are optimized starting from the value from column (b).

	(a) Average of 49 runs without noise	(b) Distribution of 49 runs without noise
$\chi_P{}^2$	1.106	1.210 ± 0.058
$\chi_{BC}{}^2$	1.083	1.118 ± 0.043
^{8}B	12.72 ± 0.31	(12.7 ± 2.4) ± (2.20 ± 0.10)
^{10}C	2.25 ± 0.04	(2.26 ± 0.26) ± (0.28 ± 0.01)
^{15}O	0.90 ± 0.03	(0.90 ± 0.23) ± (0.230 ± 0.005)
^{11}C	0.61 ± 0.02	(0.61 ± 0.11) ± (0.110±0.002)
^{9}C	22.8 ± 2.1	(23 ± 15) ± (14.6 ± 0.9)

	(c) MC with noise with 5 parameters	(d) MC with noise with 3 parameters	(e) Experimental with 3 parameters
$\chi_P{}^2$	1.220 ± 0.075	1.220 ± 0.075	1.181
$\chi_{BC}{}^2$	1.010±0.045	1.015 ± 0.045	1.008
^{8}B	(12.7 ± 3.0) ± (2.90 ± 0.10)	(12.8 ± 2.5) ± (2.14 ± 0.07)	13.6 ± 2.3
^{10}C	(2.30 ± 0.50) ± (0.535 ± 0.005)	(2.27 ± 0.31) ± (0.300±0.003)	3.74 ± 0.32

8

^{15}O	$(0.85 \pm 0.52) \pm (0.525 \pm 0.005)$	*0.9*	*0.9*
^{11}C	$(0.64 \pm 0.26) \pm (0.265 \pm 0.002)$	$(0.61 \pm 0.07) \pm (0.065 \pm 0.001)$	0.605 ± 0.065
^{9}C	$(24 \pm 18) \pm (17.0 \pm 1.0)$	*22.5*	*22.5*

By comparing the experimental data with the simulated ones, the quality of the fit corroborates the choice of fixing parameters for the two isotope ^{15}O and ^{9}C. Moreover, by comparing the figures of column (e) with the ones of column (a) one can conclude that, within the errors, the contributions of ^{8}B and ^{11}C agree with MC predictions, while FLUKA underestimates the ^{10}C contribution by a factor 1.65 ± 0.15, which is closed to the factor 2 mentioned in Battistoni et al.[9]

Experimental images and profiles along the beam direction.

As a first result of the second analysis, the reconstructed PET images, after a 0.6 s irradiation time with $3 \cdot 10^7$ ions and with applied energy cuts and median filter, are presented in Figure 5 in time intervals of 2, 4, 8, 10, 12, 24 seconds.
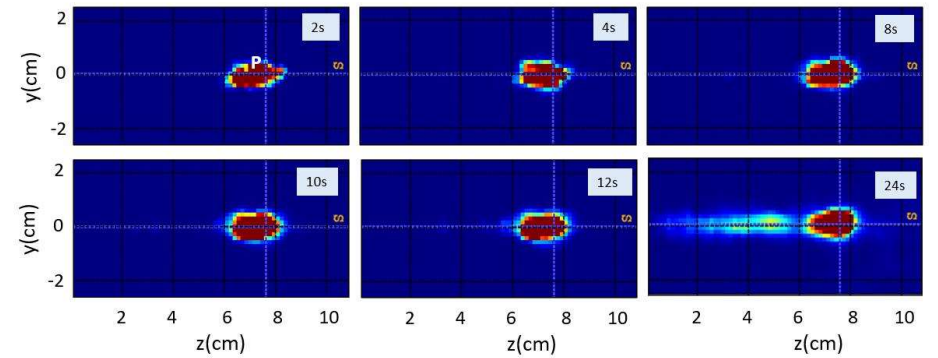

Figure 5. *2D maps of the measured PET coincidences reconstructed with MLEM algorithm and applying the median filter in time interval equal to 2, 4, 8, 10, 12, 24 s after the end of the irradiation. (Images normalized to their maximum value).*

In Table 3 the intensity J of the images in figure 5, in the point P (i.e. the crossing of the two dashed lines) is expressed in arbitrary units (a.u.).

Table 3. The intensity J in the point P of the images in figure 5 and figure 1

t (s)	*2*	*4*	*8*	*10*	*12*	*24*	*231*
J(a.u.) in P	0.01	0.13	0.86	1.07	1.41	4.65	$3.30 \ 10^4$

Although the intensity is different, the images in figure 5 show that, by reducing the acquisition time, still the region with the maximum intensity of the signal is always the same.

With reference to Figure 6, the red curve represents the longitudinal profile (laterally integrated) of the image along the z axis reconstructed from -231 s data acquisition; the FLUKA prediction, obtained from the sums of the 49 simulations and normalized to the peak value, is shown in black. The excess in the experimental curve is not fully understood but is irrelevant for the rest of this study; it could be due to a residual lutetium background not properly discarded by the median filter.
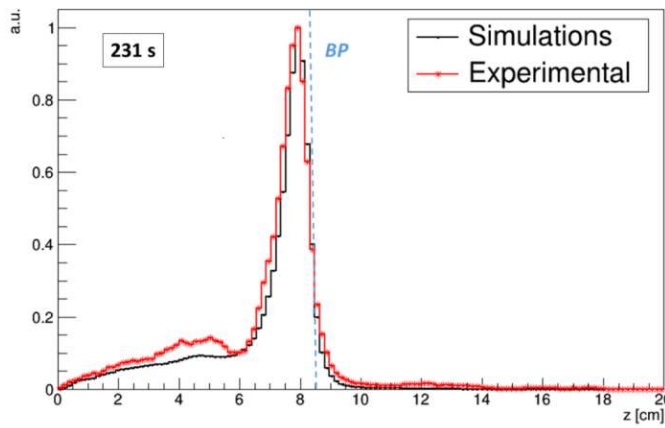

Figure 6. *Longitudinal 1D profiles of the reconstructed images at 231 s for the experimental (red) and MC simulated (black) data. The vertical dotted line represents the expected position (85.0 mm) of the Bragg Peak (BP) at 222 MeV/u in PMMA.*

Figure 7 shows the comparison of the longitudinal 1D profiles of the images reconstructed from the events collected in 2, 4, 8 10, 12, 24 s and the corresponding FLUKA predictions. The conclusions are that, the contribution from long-lived target fragmentation radionuclei is not significant at early times -and that, in the range 8-12 s, the MC reproduces the z-dependence of the experimental data with a normalization factor of about 2.5 (sim/exp).
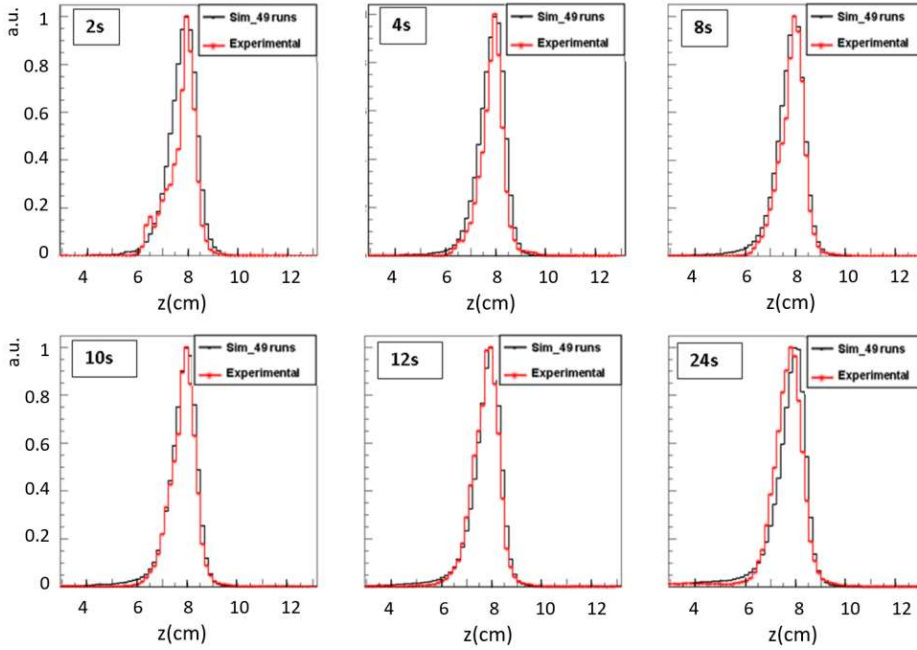
10

Figure 7. *Comparison between Fluka MC simulations (black) and experimental results (red) of longitudinal activity profiles reconstructed from events collected in 2, 4, 8, 10, 12, 24 s. The results in z axis are shown in the range 3 -13 cm, the target starts in z=0. The MC results are normalized to the experimental data at the peak. The normalization factor is about 2.5 (sim/exp).*

The agreement between the simulated and the experimental profiles can be quantified by comparing the parameters of their Gaussian fits, as shown in Table 4.

Table 4. Comparison between the Gaussian parameters in simulated and experimental data for different acquisition times. The errors are 1-σ values from the 49 MC runs.

Fitted parameters	Acquisition time (s)						
	2	**4**	**6**	**8**	**10**	**12**	**24**
z_{mean} (mm) *sim.*	*76.5±2.6*	*76.9±1.2*	*76.7±1.0*	*76.8±0.7*	*77±0.7*	*76.9±0.7*	*77.1±0.5*
z_{mean} (mm) exp.	77.0	76.8	76.9	77.2	76.7	76.1	75.6
σ_{peak} (mm) *sim.*	*4.6±1.8*	*4.3±0.6*	*4.4±0.6*	*4.3±0.5*	*4.3±0.4*	*4.4±0.4*	*4.5±0.3*
σ_{peak} (mm) exp.	4.0	3.9	4.5	4.4	4.3	4.4	4.8

The excellent agreement demonstrates that the FLUKA MC simulations can accurately predict the PET activity peak and its uncertainties.

11

As a further step towards the determination of the accuracy with which the centre of the *z*-distribution can be determined, figure 8 shows the longitudinal activity profile distribution of 6 runs of FLUKA Monte Carlo reconstructed from simulated events acquired in 8 s. The numbers of coincidences for each run are shown in the insets.
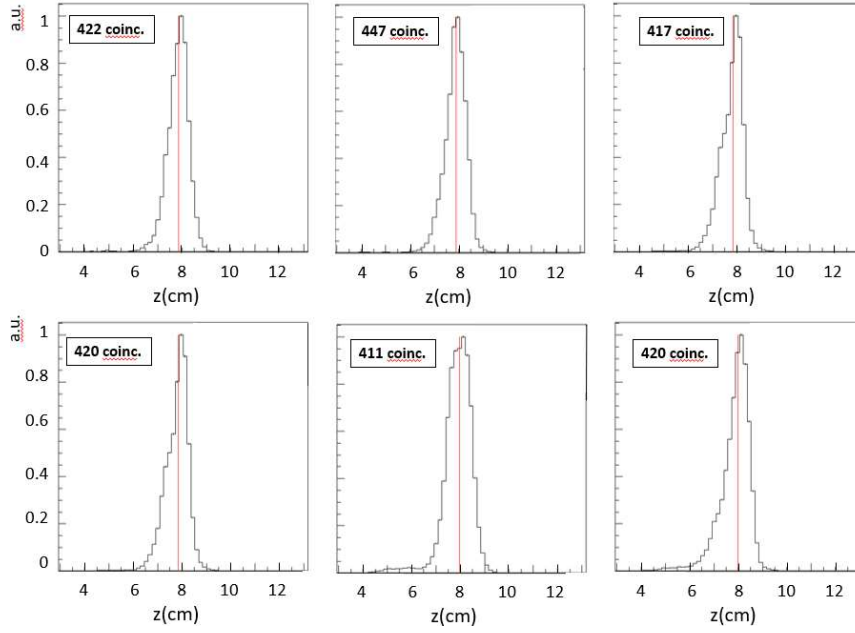

Figure 8. *Longitudinal activity profile of six of the 49 runs of FLUKA MC simulations reconstructed from events acquired in the first 8s and $3 \cdot 10^7$ carbon ions. The red lines represent the mean values of the Gaussian fits. The numbers of coincidences for each run are shown in the insets.*

Figure 9 gives, for the 49 MC runs, the distribution of z_{mean} at 8 s, i.e. the fitted mean value of each simulation run *i*, and shows a Gaussian shape with a mean value of 76.8 mm and a sigma equal to 0.7 mm, as indicated in Table 4. Since the carbon ion beam range is 85.0 mm (Figure 6) to compute it one has to add (85.0 – 76.8) = 8.2 mm to the measured position of the PET peak.
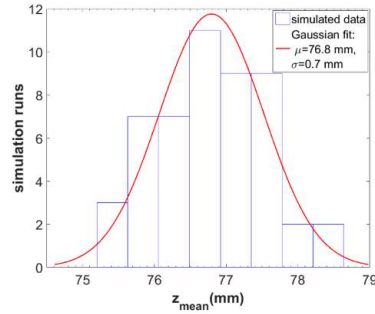
Figure 9. *Distribution at 8 s of the mean values z_{mean} of 49 MC runs . The Gaussian fit has a mean $\mu= 76.8$ mm and a standard deviation $\sigma= 0.7$ mm.*

Both the measured position of the peak z_{mean} and the width of the activity peak σ_{Peak} are found to be compatible with the corresponding quantities from the simulated runs, as shown in Table 4. Finally, as shown in Figure 10, the sigma value of the Gaussian fit of z_{mean} ($\sigma_{z\ mean}$) reduces as $1/\sqrt{t}$ with the increasing of number of coincidences, ~~as expected from Poisson's statistics, describing this process.~~ The Poissonian nature of the decay process implies that $\sigma_{z\ mean}$ scales with $1/\sqrt{N}$, where N is the number of coincidences, which in turn scales (almost) linearly with time (t), leading to a $1/\sqrt{t}$ dependence (Figure 10 right)[3]. The fitted red curve proves that, with an acquisition time of 6 s, the range can be determined with a precision of 1 mm.
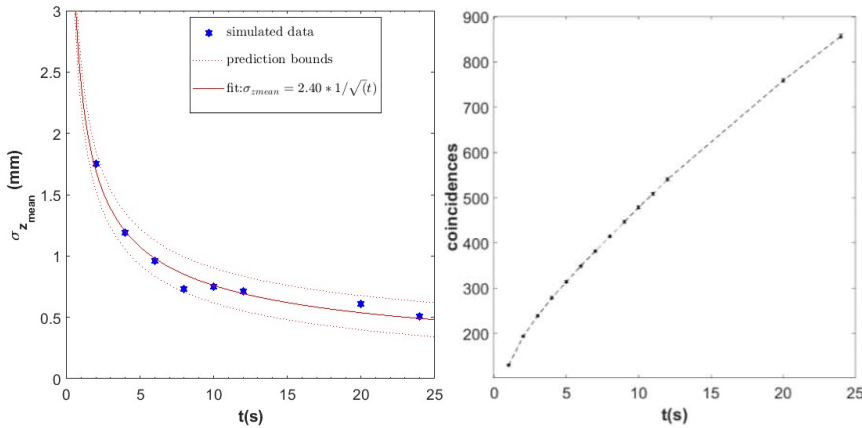

Figure 10. *Left: Standard deviation, σ_{z_mean}, values obtained from the Gaussian fit of z_{mean} –function of acquisition times: 2, 4, 6, 8, 10, 12, 20, 24 s. The best fitting curve is proportional to $1/\sqrt{t}$. Prediction bounds at 95% confidence level are also shown. Right: time-dependence of the number of coincidences in the whole target.*

---

[3] Indeed in the first 24 s, this quasi-linear trend can be understood from Figure 2 right, where the single contribution to the total counts is presented: the ^{8}B, decaying quickly, give a constant contribution to the final count curve, the ^{11}C and ^{15}O, having longer half-life, give a linear contribution, instead for ^{10}C the $1- e^{-\lambda t}$ contribution is still dominant.

4. Discussion

A PMMA homogeneous phantom was irradiated at CNAO with ^{12}C ion beams at 222 MeV/u for 0.6 s half second and the 3D-PET signal over time was collected by the INSIDE detector. Although similar experiments were performed with INSIDE at CNAO [12], this was the first time that such a short ^{12}C irradiation was performed and analysed. In this paper, a detailed analysis of the acquired PET signal has been presented in order to extract the contributions of the main isotopes (^{8}B and ^{10}C, detectable at short acquisition times, ^{15}O and ^{11}C which start to dominate at longer time) and and quantify the error in the measurement of the carbon ion beam range.

The INSIDE double head PET detector registered, without energy filter, 15700 coincidences in 231 s. In this number, the intrinsic LFS-related random background is included. From the experimental runs with no beam the background noise rate has been measured to be (51.0±0.9) coincidences/s, corresponding to 11800 in 231 s, which leaves a signal of 3900 true coincidences, only 25 % of the total number of coincidences. With the energy filter, the total number of coincidences in 231 s is about 5600 and the background noise rate decreases by a factor of 4, corresponding to about 2800 coincidences in 231 s (i.e. about 70% of true coincidences without energy filter). The number of true coincidences in this case increases to 50 % of the total number of coincidences.

Despite the luthetium background, the results collected in Table 4 show that in a few seconds it is possible to reconstruct a Gaussian-shaped activity distribution with FWHM $\simeq$ 10 mm along the beam direction, coming from the short-lived β^+ emitters fragments of the ^{12}C projectiles.

The analysis of experimental and of the FLUKA MC simulated coincidences as a function of time has shown that for the short acquisition times considered ^{8}B and ^{10}C are the main contributors to the very narrow and clear peaks shown in Figures 7 and 8. Although the INSIDE detector has not been optimized for measurement of cross-sections, fitting analysis suggests an underestimation of the ^{10}C production with respect to ^{8}B in the FLUKA version used in this work. This factor has been quantified in this analysis to be about 60%.

In addition, as confirmed by 49 runs of FLUKA simulations, performed in the same experimental scenario, the statistical contribution given by the low number of coincidences accounts for 1 mm for a measurement time of about 6 s. As shown in Figure 10, with a 10 s calibration run the standard deviation can be reduced to 0.75 mm.

It is worth mentioning that promising results have already been obtained with INSIDE in clinical scenarios using inter-spill data at CNAO [12], but the development of a dedicated synchronization system, based on CNAO synchrotron time structure was required. The new rapid range verification, PET-based method could be included in the panorama of other emerging monitoring techniques during hadron therapy, such as prompt photons imaging [30] [31], combined PET and prompt -gammas techniques [32,33] and charged secondaries techniques [34] [35].

In particular, the method could be performed with a two-head detector with any type of ion accelerator, following the approach chosen in this work.

In order to give a low dose (for instance 0.2 Gy) during this calibration run that typically will precede the irradiation run, the spot can be moved along a 3-5 cm segment located at the center of the tumor and aligned along the axis of the PET detector. The result, computed on-line, can then be used to correct the carbon ion beam range during the much longer irradiation run by applying a correction to the Treatment Plan that considers the small dose due to the calibration run.

14

5. Conclusions

Some years ago two of us proposed a method for verifying the range in carbon ion therapy by using short-lived positron emitters from a pre-irradiation short, low dose run on a small part of the tumor target. The method does not depend on the time structure of the accelerator and on complex synchronization systems.

The validity of the method has been verified by experiments performed with the INSIDE detector at CNAO, the Italian Centre for Oncological Hadron Therapy in Pavia. In this paper the detailed PET analysis of an experiment performed at 222 MeV/u with $3 \cdot 10^7$ carbon ions impinging for 0.6 s on a PMMA homogeneous phantom has been presented.

The comparison of the measured longitudinal β^+ activity distributions with the predictions of 49 runs of complete FLUKA simulations resulted in four main conclusions:

- the time dependence of the measured activity, in the 24 seconds that follow the 0.6 s irradiation, agrees quantitatively with the expected one, once ~~added~~ the lut~~h~~etium background is added to the simulation;

- the time-fit shows that the main contribution of ^8B is well predicted by FLUKA while the ^{10}C yield is 60% larger than the prediction, most probably due to an underestimate of the production cross-section;

- once the median filter is applied to the data, the longitudinal z-distributions of the activities in ~~in~~ 2, 4, 8, 10, 12 and 24 seconds are almost Gaussian distributions with FWHM $\simeq$ 10 mm, in good agreement with FLUKA predictions.

- from the distribution of the average peak positions of 49 FLUKA runs it can be concluded that, with an acquisition time of 6 s, the carbon ion beam range can be determined with a precision of σ = 1 mm by adding 8.2 mm to the fitted position of the PET signal peak; with a 10 s calibration run the sigma can be reduced to 0.75 mm.

Further studies are needed at different energy values of the primary beam in order to assess the impact of the different fractions of fragments production and in more complex experimental scenarios, in order to consider for example the inhomogeneities of a real target. However this work opens an interesting perspective for the in-vivo range verification during a patient treatment.

6. Acknowledgments

15

7. References

[1] Enghardt W, Debus J, Haberer T, Hasch BG, Hinz R, Jäkel O, et al. Positron emission tomography for quality assurance of cancer therapy with light ion beams. Nucl Phys A 1999;654:1047c–50c. https://doi.org/10.1016/S0375-9474(00)88597-8.

[2] J. Pawelke WE. In-Beam PET Imaging for the Control of Heavy-Ion Tumour Therapy. IEEE 1997.

[3] Parodi K. Vision 20/20: Positron emission tomography in radiation therapy planning, delivery, and monitoring. Med Phys 2015;42:7153–68. https://doi.org/10.1118/1.4935869.

[4] Darafsheh A. Radiation Therapy Dosimetry: A Practical Handbook. CRC Press; 2021.

[5] Hünemohr N, Krauss B, Dinkel J, Gillmann C, Ackermann B, Jäkel O, et al. Ion range estimation by using dual energy computed tomography. Z Med Phys 2013;23:300–13. https://doi.org/10.1016/J.ZEMEDI.2013.03.001.

[6] Cuccagna C, Augusto RS, Kozlowska W, Ortega PG, Vlachoudis V, Ferrari A, et al. Evaluation study of in-beam PET performances with a Carbon ion linac (CABOTO). Radiotherapy and Oncology 2016;118:S28–9. https://doi.org/10.1016/S0167-8140(16)30058-5.

[7] Augusto RS, Bauer J, Bouhali O, Cuccagna C, Gianoli C, Kozłowska WS, et al. An overview of recent developments in FLUKA PET TOOLS. Physica Medica 2018;54:189–99. https://doi.org/10.1016/j.ejmp.2018.06.636.

[8] Ferrari A, Sala PR, Fasso A, Ranft J. FLUKA: A multi-particle transport code (Program version 2005) 2005.

[9] Battistoni G, Bauer J, Boehlen TT, Cerutti F, Chin MPW, Dos Santos Augusto R, et al. The FLUKA Code: An Accurate Simulation Tool for Particle Therapy. Front Oncol 2016;6:116. https://doi.org/10.3389/fonc.2016.00116.

[10] Ferrero V. The INSIDE project: in-beam PET scanner system features and characterization. Journal of Instrumentation 2017;12:C03051–C03051. https://doi.org/10.1088/1748-0221/12/03/C03051.

[11] Bisogni MG, Attili A, Battistoni G, Belcari N, Camarlinghi N, Cerello P, et al. INSIDE in-beam positron emission tomography system for particle range monitoring in hadrontherapy. J Med Imaging (Bellingham) 2017;4:011005. https://doi.org/10.1117/1.JMI.4.1.011005.

[12] Pennazio F, Battistoni G, Bisogni MG, Camarlinghi N, Ferrari A, Ferrero V, et al. Carbon ions beam therapy monitoring with the INSIDE in-beam PET. Phys Med Biol 2018;63:145018. https://doi.org/10.1088/1361-6560/aacab8.

[13] Fiorina E. An integrated system for the online monitoring of particle therapy treatment accuracy. Nucl Instrum Methods Phys Res A 2016;824:198–201. https://doi.org/10.1016/J.NIMA.2015.11.029.

16

[14] Piliero M A, Pennazio F, Bisogni MG, Camarlinghi N, Cerello PG, Del Guerra A, et al. Full-beam performances of a PET detector with synchrotron therapeutic proton beams. Phys Med Biol 2016;61:N650–66. https://doi.org/10.1088/0031-9155/61/23/N650.

[15] Camarlinghi N, Sportelli G, Battistoni G, Belcari N, Cecchetti M, Cirrone GAP, et al. An in-beam PET system for monitoring ion-beam therapy: test on phantoms using clinical 62 MeV protons. Journal of Instrumentation 2014;9:C04005. https://doi.org/10.1088/1748-0221/9/04/C04005.

[16] Justusson BI. Median filtering: statistical properties. Two-Dimensional Digital Signal Processing II 1981:161–96. https://doi.org/10.1007/bfb0057597.

[17] Zhu Y, Huang C. An Improved Median Filtering Algorithm for Image Noise Reduction. Phys Procedia 2012;25:609–16. https://doi.org/10.1016/j.phpro.2012.03.133.

[18] Yushkevich PA, Piven J, Hazlett HC, Smith RG, Ho S, Gee JC, et al. User-guided 3D active contour segmentation of anatomical structures: Significantly improved efficiency and reliability. Neuroimage 2006;31:1116–28. https://doi.org/10.1016/j.neuroimage.2006.01.015.

[19] Fiorina E, Ferrero V, Pennazio F, Baroni G, Battistoni G, Belcari N, et al. Monte Carlo simulation tool for online treatment monitoring in hadrontherapy with in-beam PET: A patient study. Phys Med 2018;51:71–80. https://doi.org/10.1016/j.ejmp.2018.05.002.

[20] Sorge H, Stöcker H, Greiner W. Poincaré invariant Hamiltonian dynamics: Modelling multi-hadronic interactions in a phase space approach. Ann Phys (N Y) 1989;192:266–306. https://doi.org/10.1016/0003-4916(89)90136-X.

[21] Cerutti F, Battistoni G, Capezzali G, Colleoni P, Ferrari A, Gadioli E, et al. Low energy nucleus–nucleus reactions: the BME approach and its interface with FLUKA. Proc 11th Int Conf on Nuclear Reaction Mechanisms (Varenna, Italy) 2006.

[22] Cerutti F, Dosanjh M, Ferrari A, Mendonca T, Ortega PG, Parodi K, et al. A systematic Monte Carlo study on the dosimetric and imaging properties of C-11 and O-15 beams. Radiotherapy and Oncology 2016;118:S5. https://doi.org/10.1016/S0167-8140(16)30011-1.

[23] Kozłowska WS, Böhlen TT, Cuccagna C, Ferrari A, Fracchiolla F, Magro G, et al. FLUKA particle therapy tool for Monte Carlo independent calculation of scanned proton and carbon ion beam therapy. Phys Med Biol 2019;64. https://doi.org/10.1088/1361-6560/ab02cb.

[24] Brun R, Rademakers F. ROOT - An object oriented data analysis framework. Nucl Instrum Methods Phys Res A 1997;389:81–6. https://doi.org/10.1016/S0168-9002(97)00048-X.

[25] Mathworks Inc. MATLAB version 8.5.0.197613 (R2015a) 2015.

[26] Wei Q. Intrinsic Radiation in Lutetium Based PET Detector: Advantages and Disadvantages. Chinese Physics C Supported by China Postdoctoral Science Foundation 2014.

[27] James F. Statistical Methods in Experimental Physics. WORLD SCIENTIFIC; 2006. https://doi.org/10.1142/6096.

[28] Dr. Olaf Behnke DrKKDrGSDrTS-S. Data Analysis in High Energy Physics. Weinheim, Germany: Wiley-VCH Verlag GmbH & Co. KGaA; 2013. https://doi.org/10.1002/9783527653416.

[29] Baker S, Cousins RD. Clarification of the use of CHI-square and likelihood functions in fits to histograms. Nuclear Instruments and Methods In Physics Research 1984;221:437–42. https://doi.org/10.1016/0167-5087(84)90016-4.

[30] Missaglia A, Bourkadi-Idrissi A, Casamichiela F, Mazzucconi D, Carminati M, Agosteo S, et al. Prompt-gamma fall-off estimation with C-ion irradiation at clinical energies, using a knife-edge slit camera: A Monte Carlo study. Physica Medica 2023;107:102554. https://doi.org/10.1016/j.ejmp.2023.102554.

[31] Yamamoto S, Yabe T, Akagi T, Yamaguchi M, Kawachi N, Kamada K, et al. Prompt X-ray imaging during irradiation with spread-out Bragg peak (SOBP) beams of carbon ions. Physica Medica 2023;109:102592. https://doi.org/10.1016/j.ejmp.2023.102592.

[32] Ferrero V, Cerello P, Fiorina E, Monaco V, Rafecas M, Wheadon R, et al. Innovation in online hadrontherapy monitoring: An in-beam PET and prompt-gamma-timing combined device. Nucl Instrum Methods Phys Res A 2018. https://doi.org/10.1016/J.NIMA.2018.08.065.

[33] Pennazio F, Ferrero V, D'Onghia G, Garbolino S, Fiorina E, Marti Villarreal OA, et al. Proton therapy monitoring: spatiotemporal emission reconstruction with prompt gamma timing and implementation with PET detectors. Phys Med Biol 2022;67:065005. https://doi.org/10.1088/1361-6560/ac5765.

[34] Battistoni G, Collamati F, De Lucia E, Faccini R, Marafini M, Mattei I, et al. Design of a tracking device for on-line dose monitoring in hadrontherapy. Nucl Instrum Methods Phys Res A 2017;845:679–83. https://doi.org/10.1016/j.nima.2016.05.095.

[35] Traini G, Mattei I, Battistoni G, Bisogni MG, De Simoni M, Dong Y, et al. Review and performance of the Dose Profiler, a particle therapy treatments online monitor. Physica Medica 2019;65:84–93. https://doi.org/10.1016/J.EJMP.2019.07.010.

18